Dynamic effects of quenched disorder on domain wall motion in magnetic nanowires

Y. Y. He,[1] B. Zheng,[1,*] and N. J. Zhou[2]

[1]*Department of Physics, Zhejiang University, Hangzhou 310027, People's Republic of China*
[2]*Department of Physics, Hangzhou Normal University, Hangzhou 310036, People's Republic of China*

The domain wall dynamics in magnetic nanowires is numerically studied with the Landau-Lifshitz-Gilbert equation. Below the Walker breakdown threshold, the domain wall presents a stable propagation, while above the threshold where the retrograde mode dominates, the oscillation period is controlled by the external field and anisotropy. More importantly, the dynamic effects of quenched disorder on the domain wall motion are explored. A continuous pinning-depinning phase transition is detected. The dynamic scaling form is analyzed with the data collapse of the domain wall velocity, and both the static and dynamic critical exponents are extracted.

I. INTRODUCTION

In the study of low-dimensional magnetic materials during the past decade, much attention has been attracted in the domain wall dynamics due to the potential applications in data storage and logic devices [1–3]. The precisely controlled domain wall displacement is a prerequisite for the operations, thus a thorough theoretical investigation is required of the domain wall dynamics, especially that governed by the Landau-Lifshitz-Gilbert (LLG) equation. Recent efforts have led to some theoretical solutions in limiting cases, e.g., with the assumption of small driving fields and the restriction of spin motion to be almost in one plane [4–6]. There are experimental evidences for the existence of the Walker threshold [7,8], but the validity of the Walker theory varies under different conditions [9–13]. Succedent research has revealed that by the influence of spin waves on the domain wall propagation, the simulation results deviate from the Walker theory if the external field is in a certain regime below the Walker breakdown threshold [14].

The retrograde breathing motion of a domain wall beyond the Walker breakdown threshold is also analyzed, whereas the theoretical solutions of the domain wall displacement and oscillation period only exist without the Gilbert damping [15], or with an approximation of the uniaxial magnetic anisotropy [16]. The lack of numerical evidence indicates that the understanding of the retrograde breathing behavior is incomplete [17].

More importantly, various pinning effects are also significant in manipulating the domain wall movement in a magnetic nanowire. It is the numerical and experimental facts that thickness inhomogeneities and geometrical constrictions can pin a domain wall, and the depinning field depends on the geometry of the material structures [18–21]. For instance, the domain wall pinning in a notched magnetic wire can be understood in a unified approximate theory [22], but the criterion for the existence of a domain wall solution is not yet known.

In particular, the domain wall motion described by the LLG equation with quenched disorder remains a conundrum.

In the past years, supported by the results from experiments [23,24], the usual numerical analysis on the phase transitions of the domain wall motion in ferromagnetic materials is typically based on the Monte Carlo simulation, Edwards-Wilkinson equation with quenched disorder (QEW), and Hamiltonian equation of the ϕ^4 theory [25–33]. The pinning and depinning phases of the domain wall motion governed by the LLG equation have been recently observed [34–36], and the transition field in Tb/Co multilayer wires is linearly dependent on the injecting current in experiments [37]. However, a deep analysis on the possible phase transition is still lacking. In this paper, we detect a continuous transition between the pinning and depinning phases, especially with focus on analyzing the dynamic scaling behavior and measuring the dynamic and static critical exponents.

This paper is organized as follows. We give a description of the magnetic model governed by the LLG equation in Sec. II and present the simulation results of the domain wall motion in a magnetic nanowire in Sec. III. In Sec. IV we study the dynamic effects of quenched disorder in the domain wall motion, with focus on the pinning-depinning phase transition and the dynamic scaling behavior. The summary is included in Sec. V.

II. THE MODEL

We consider a classical Heisenberg model with an anisotropy on an one-dimensional (1D) lattice chain with the Hamiltonian

$$\mathcal{H} = -J \sum_{\langle ij \rangle} \mathbf{S}_i \cdot \mathbf{S}_j + D_\perp \sum_i S_{i,z}^2$$
$$- D_\parallel \sum_i S_{i,x}^2 - M_s \sum_i (\mathbf{H} + \mathbf{h}_i) \cdot \mathbf{S}_i, \quad (1)$$

where $\mathbf{S}_i$ is a three-dimensional magnetic moment of unit length, and $\langle ij \rangle$ denotes the sum over the nearest neighbors. The hard z-axis anisotropy regulated by a positive $D_\perp$ favors an easy xy plane, while a positive $D_\parallel$ describes the easy x axis. M_s is the saturation magnetization, $\mathbf{H}$ is a constant external magnetic field, and $\mathbf{h}_i$ stands for the random field on each magnetic moment.

---
*zhengbo@zju.edu.cn
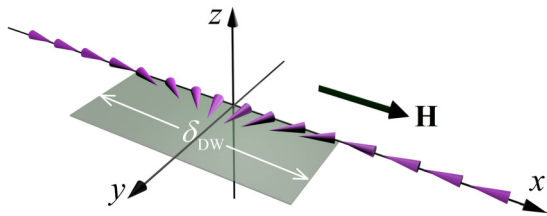
FIG. 1. A 1D head-to-head domain wall in a nanowire. δ_{DW} denotes the domain wall width. **H** is a constant external magnetic field along the x axis, which is considered to be the easy axis.

The dynamics of the spin model is described by the LLG equation,

$$\frac{\partial \mathbf{S}_i}{\partial t} = -\gamma \mathbf{S}_i \times \mathbf{H}_i^{\mathrm{eff}} + \alpha \left(\mathbf{S}_i \times \frac{\partial \mathbf{S}_i}{\partial t} \right), \quad \mathbf{H}_i^{\mathrm{eff}} = -\frac{\partial \mathcal{H}}{\partial \mathbf{S}_i}. \quad (2)$$

Here $\mathbf{H}_i^{\mathrm{eff}}$ is the effective magnetic field, γ denotes the gyromagnetic ratio, and α is the dimensionless Gilbert damping constant. If the temperature is above zero, the pinning-depinning phase transition usually softens [26]. In this paper, we only consider the magnetic system at zero temperature.

For a cylindrical system whose diameter is smaller than the exchange length of the given magnetic material, or in other words, for a quasi-1D system, the exchange interaction dominates the stray field energy induced by the magnetic charges on the edges. Thus, the system behaves effectively as one-dimensional under certain conditions, e.g., for the transverse domain wall, where the structure tends to be homogeneous in the transverse direction [17,38]. Nevertheless, other quasi-1D systems such as the vortex domain wall may behave differently from the 1D system [39], and this issue requires further study.

In this paper, we numerically solve the LLG equation on a 1D nanowire with the length of $L = 20\,000$ lattice sites and an antiperiodic boundary condition. The initial configuration is shown in Fig. 1. Longer wires with $L = 40\,000$ and $80\,000$ are also used to avoid the finite-size effects, in case the domain wall moves faster under a stronger external field. Besides, the spin waves exist as a typical phenomenon of the LLG equation [14]. They propagate much faster than the domain wall and reflect when crossing the boundaries. The results from simulations with $L = 40\,000$ and $80\,000$ are consistent so that the boundary effects resulted by the spin waves are negligible.

The initial domain wall width is set to be $\delta_{\mathrm{DW}} = \pi \sqrt{A/K_\parallel}$, with the exchange constant $A = 3.84 \times 10^{-12}$ J/m, the easy axis coefficient $K_\parallel = 2 \times 10^3$ J/m^3, following the electric insulator yttrium iron garnet (YIG) [14,40]. The time, length, and energy density are measured in units of $(\gamma M_s)^{-1}$, δ_{DW}, and $\mu_0 M_s^2$, respectively, with $\gamma = 3.51 \times 10^4$ m/(A $\cdot$ s) and $M_s = 1.94 \times 10^5$ A/m. The exchange and anisotropy coefficients in Eq. (1) are unitized as $J = A/(\mu_0 M_s^2 a^2) = 52.8$, $D_\parallel = K_\parallel/(\mu_0 M_s^2) = 0.0423$, and $D_\perp = K_\perp/(\mu_0 M_s^2)$, with $a = 1.24$ nm according to the YIG lattice constant [14]. In this paper, the Gilbert damping constant α and the anisotropy constant $D_\perp$ are treated as adjustable parameters. The external field **H** and the random field $\mathbf{h}_i$ are presented in unit of $0.001 M_s$ for convenience.

The domain wall is initially centered on the nanowire with two domains of opposite orientations on both sides. The simulation starts by switching on a driving magnetic field **H** along the easy-x axis as shown in Fig. 1. During the dynamic evolution, the domain wall may propagate and fluctuate. There may be different definitions for the height function of the domain wall [25,29,41], and we use the relatively standard one [25,29],

$$h(t) = \frac{1}{2} \cdot \frac{a}{\delta_{\mathrm{DW}}} \sum_i S_{i,x}(t). \quad (3)$$

Here $h(t)$ indicates the effective displacement of the domain wall denoted by $x_{\mathrm{DW}}(t)$, and the length is measured in unit of δ_{DW}. The velocity of the domain wall is then calculated by

$$v(t) = \left\langle \frac{dh(t)}{dt} \right\rangle, \quad (4)$$

where $\langle ... \rangle$ denotes the statistical average. Without the quenched disorder, an equivalent definition of the domain wall displacement $x_{\mathrm{DW}}(t)$ is the location of the minimal $S_{i,x}$ [41].

III. OSCILLATION PERIOD WITHOUT QUENCHED DISORDER

In this section, we consider the case of a zero random field, i.e., $\mathbf{h}_i = 0$ in Eq. (1). According to the theoretical deduction by Walker [4], under the assumption that $\mathbf{S}_i$ is only a function in z axis, the domain wall may either reach a stable state with a constant velocity when the driving field $H = |\mathbf{H}|$ is below the Walker breakdown threshold H_{WB}, or shift to a retrograde breathing mode with periodical oscillations when H is above H_{WB} [6,10,14,41].

In the past years, numerical study of the domain wall propagation usually elides the small regime around H_{WB} and analyzes the domain wall dynamics below and above H_{WB} with different principles [6,41]. Some numerical results deviate from the rigid Walker theory when H is in a certain regime, $H_{\mathrm{M}} < H < H_{\mathrm{WB}}$, $H_{\mathrm{M}} \approx 2(D_\parallel/D_\perp)^{0.25} H_{\mathrm{WB}}$ [10,14]. An obscure explanation is that as long as the domain wall propagates, the spin wave presents as the local modulation that radiates away from the domain wall center, yet this phenomenon is absent in the Walker theory. The Gilbert damping abates the spin-wave emission and disturbs the stable propagation of the domain wall for $H > H_{\mathrm{M}}$ [14]. Nevertheless, we enlarge the lattice and prolong the simulation time until the domain wall motion reaches a steady state, and our study explores more accurate results that support the Walker theory in the entire regime below H_{WB} [42]. In the computations, we use the fourth-order Runge-Kutta method and Gauss-Seidel-projection method for comparison [43], and both methods lead to the same result.

Although the approximate theoretical solutions below the Walker breakdown threshold have been studied in various cases, with the assumptions of an uniaxial anisotropy, small damping coefficients, or small driving fields, etc. [4–6,17], the domain wall dynamics with driving fields above the threshold remains a conundrum. The hybrid of the domain wall mobility and spin-wave emission causes an obstacle in deducing a general solution of the domain wall motion. The analysis of the relation between the oscillation period and external field
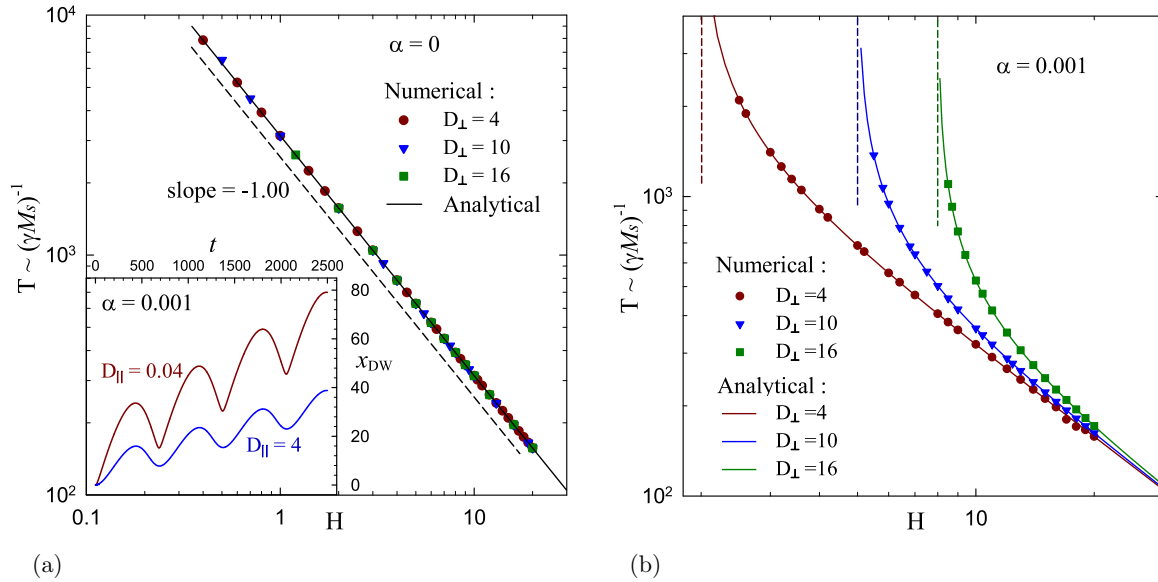
FIG. 2. The relation between H and T with different hard axis coefficients is shown on a double-log scale. (a) For $\alpha = 0$, the simulation results conform with $T = \pi/H$. The inset displays the time dependence of the domain wall displacement with $D_\parallel = 0.04$ and 4, respectively, while $\alpha = 0.001$ and $D_\perp = 4$ are fixed parameters. (b) For $\alpha = 0.001$, the simulation results are compared with the theoretical expression in Eq. (5), and the vertical short dashed lines mark the values of H_{WB} as $T \to \infty$.

may contribute to the understanding of the domain wall motion for $H > H_{\mathrm{WB}}$. In the past decade, some theoretical study has deduced the solution of the oscillation period [15,16], yet there is an approximation in the uniaxial magnetic anisotropy or an assumption of zero damping. In order to understand deeper how to control the oscillation period, we consider the biaxial anisotropy and perform relevant numerical simulations.

Without the Gilbert damping ($\alpha = 0$), one may equivalently consider H_{WB} to be zero, and the retrograde mode appears when $H > 0$. As J is much larger than $D_\perp$ in the following analysis, the domain wall retrogrades to the initial position after one period [41]. On the contrary, if J is smaller and close to $D_\perp$, the domain wall oscillates with an effective displacement. Under the assumption of a broad domain wall, i.e., $J/D_\parallel \gg 1$, the theoretical solution concludes that the oscillation period is only dependent on the driving field by $T = \pi/H$ [15], yet the easy and hard anisotropy coefficients merely affect the amplitude of oscillation. The numerical results of different $D_\perp$ in Fig. 2(a) coincide with the relation $T = \pi/H$ denoted by the solid line.

When there exists a nonzero damping factor ($\alpha > 0$), one may introduce a polar angle θ and an azimuthal angle ϕ to describe the motion of the magnetic moments in the spherical coordinate. The macroscopic retrograde motion of the domain wall is actually induced by the microscopic precession of the magnetic moments [16]. The oscillation period is therefore considered to be equivalent to the precession time of reversing the magnetic moments in the domain wall. We derive the theoretical expression of the period T as follows:

$$T = \frac{2\pi(\alpha^2 + 1)}{\sqrt{4H^2(\alpha^2 + 1) - \alpha^2 D_\perp^2}}. \qquad (5)$$

The deduction in Ref. [16] is under the assumption of the uniaxial magnetic anisotropy, in other words, $D = D_\parallel = D_\perp$.

However, according to our analysis with biaxial anisotropy ($D_\parallel \neq D_\perp$), the oscillation period is controlled by the damping factor α, the external field H, and the hard anisotropy $D_\perp$, yet the easy anisotropy $D_\parallel$ hardly affects the period. For example, we display the domain wall displacement with $D_\parallel = 0.04$ and $D_\parallel = 4$, respectively, in the inset of Fig. 2(a), the two oscillation curves comply with the same period, yet the amplitude is smaller for the larger $D_\parallel$.

In Fig. 2(b), we display the simulation results of $\alpha = 0.001$ and the theoretical curves of Eq. (5). The damping dissipates a sort of energy on top of the spin-wave emission, which is different from the case of $\alpha = 0$. If the hard anisotropy energy is stronger, the spins are more difficult to orient out of the easy plane, thus the precession time for reversing a magnetic moment is longer. In other words, T increases as $D_\perp$ is larger for $\alpha > 0$. On the other hand, the easy anisotropy coefficient $D_\parallel$ favors the spins to rotate in the easy plane, and merely affects the propagating distance of the domain wall.

One may notice that in the case of $\alpha \ll 1$, Eq. (5) indicates that the oscillation period $T \to \infty$ as $H \to \alpha\sqrt{D_\perp^2/(\alpha^2 + 1)}/2 \approx H_{\mathrm{WB}}$. In other words, if $H = H_{\mathrm{WB}}$, the domain wall exhibits a uniform stable motion without retrograding. Moreover, in the absence of the Gilbert damping ($\alpha = 0$), Eq. (5) leads to $T \to \pi/H$ and conforms to the result stated in Fig. 2(a).

IV. DOMAIN WALL MOTION WITH QUENCHED DISORDER

The impurities or lattice defects in the materials are usually considered as quenched disorders, which may result in the pinning phenomena in the propagation of the domain wall. In this section, we describe the quenched disorder in a typical and intuitive form by introducing the random field $\mathbf{h}_i$ in Eq. (1) following Refs. [28–33,44–46]. The direction of
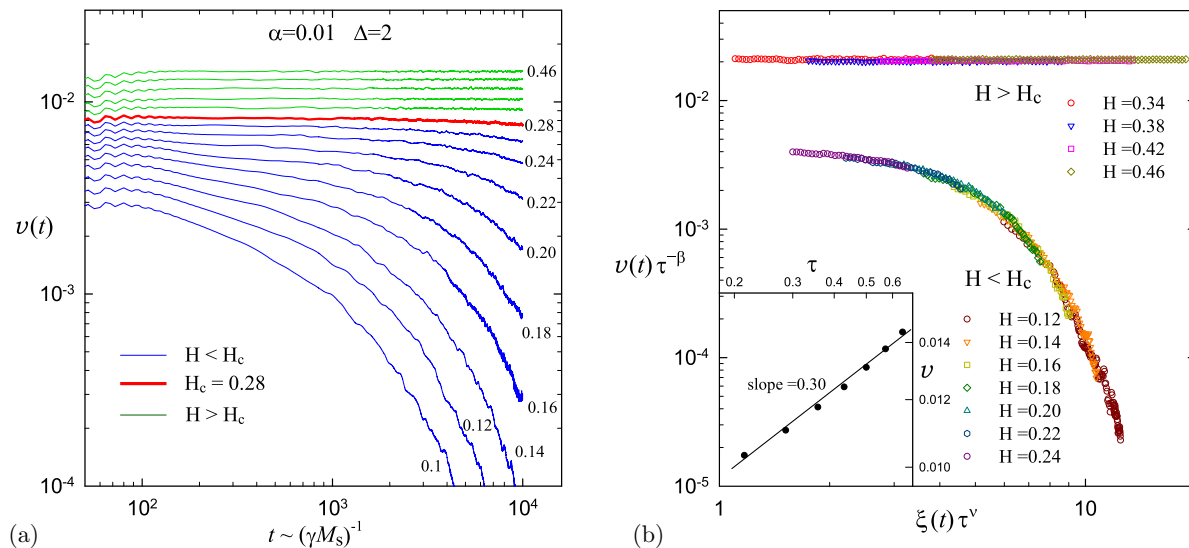
FIG. 3. (a) The domain wall velocity is shown for different H with $D_\perp = 4.23$, $\alpha = 0.01$, and $\Delta = 2$. The thin lines display the pinning state of $H < 0.28$ and depinning state of $H > 0.28$, separated by the red thick line at the transition field $H_c = 0.28$. (b) According to the dynamic scaling form in Eq. (6), the data taken from (a) are collapsed onto two curves, respectively, with H below and above the transition field. The inset displays the domain wall velocity in the steady state for $H > H_c$ on a log-log scale.

$\mathbf{h}_i$ is randomized, and the amplitude $h_i = |\mathbf{h}_i|$ is uniformly distributed within an interval $[-\Delta, \Delta]$. The disorders in other forms as random bond usually yield similar results [26]. The parameter $D_\perp = 100D_\parallel$ is fixed. The results are obtained with the statistical averages of 5 000 to 10 000 samples.

Recent numerical analysis of the pinning phenomena in nanowires governed by the LLG equation indicates that there exists a phase transition between the extrinsic pinning state and the depinning state [34], the pinning and depinning probabilities of a current-induced domain wall are also explored in experiments and numerical simulations [35,36]. However, the intrinsic nature of the phase transitions is not yet known, and the critical exponents are not measured.

Due to the influence of the disorder, the domain wall is not able to maintain the stable drilling mode of the Walker theory. For a smaller driving field H, the velocity of the domain wall presents an exponential decay after an initial rising, and finally reaches zero. This is known to be in the pinning phase. For a larger driving field H, which is above a critical value of H_c, the velocity will stabilize at a nonzero constant, which indicates that the system is in the depinning phase. When the driving field is at the critical value H_c, the dynamic system undergoes a depinning phase transition, which is intrinsically dynamic.

According to our simulations, H_c is much smaller than the Walker breakdown threshold H_{WB}, which implies that it is unable to pin the domain wall in the breathing mode for $H > H_{WB}$. We analyze the dynamic behavior of the domain wall in the pinning state for $H < H_c$, and the depinning state, i.e., the stable sliding state for $H > H_c$.

Within the microscopic timescale t_{mic}, the dynamic behavior of the domain wall velocity is nonuniversal, such as the initial rising in the very early times. The disorder in the lattice may produce local spin waves that retard the rising of the velocity within t_{mic}. But the local spin waves are weak and annihilated within a short distance, hence they hardly affect the domain wall propagation after the velocity rises

to the maximum. A larger damping constant α impedes the propagation of the spin waves, hence essentially reduces the time consumed for the rising of the velocity. We set $\alpha = 0.01$, which is larger than that used in Sec. III, and display the dynamic behavior of the domain wall velocity in Fig. 3(a). The units of Δ and H are both set to be $0.001M_s$ for convenience. The driving field H plays the role of the control parameter. In Fig. 3(a), the velocity preserves at a constant value when H is above $H_c \approx 0.28$, or displays a visible drop after an initial microscopic relaxation process when H is below H_c. Therefore, the critical driving field H_c is in the region of $(0.27, 0.29)$, thus H_c is about 0.28.

In the nonequilibrium relaxation dynamics, there may exist a dynamic scaling form [25,47], which is characterized by a growing spatial correlation length $\xi(t) \sim t^{1/z}$, with z being the dynamic critical exponent. For the domain wall dynamics, the order parameter is the domain wall velocity v, the dynamic scaling form is written as

$$v(t, \tau) = \tau^\beta F[\xi(t)\tau^\nu], \qquad (6)$$

where $\tau = (H/H_c - 1)$, β and ν are the static critical exponents. In simple words, $v(t,\tau)\tau^{-\beta}$ is controlled only by the scaling variable $\xi(t)\tau^\nu$.

With the numerical data of different H in Fig. 3(a), the data collapses are performed according to Eq. (6), respectively, for $H < H_c$ and $H > H_c$, and the results are shown in Fig. 3(b). In the computations, data up to a microscopic time scale $t_{mic} \sim 200$ are skipped. For $H < H_c$, the velocity exponentially decreases to zero, while for $H > H_c$ it remains as a constant. The data collapse includes the regimes that the driving field deviates from H_c. For H close to the critical driving field H_c, the values of τ^ν are small, thus the simulations should be performed for quite a long time to obtain a reasonable data collapse. Therefore, those data from $H = 0.26$ to 0.30 are not included in Fig. 3(b).

For $H > H_c$, the scaling function $F[\xi(t)\tau^\nu]$ in Eq. (6) is a constant, and the domain wall velocity $v \sim \tau^\beta$. In other words, the velocity is governed only by the static exponent β, and the critical exponents z and ν are actually absent in the dynamic scaling form. Thus, we may adjust H_c and β to generate a reasonable data collapse, which is shown in Fig. 3(b). The critical point H_c is estimated to be 0.28. According to our analysis, the data collapse for $H > H_c$ is quite sensitive to β. Therefore, we may confidently determine the static exponent $\beta = 0.30$ with a tolerance of ± 0.01. Alternatively, one may compute the average velocity v over time t, and plot it as a function of τ on a double-log scale as shown in the inset of Fig. 3(b). The slope of the curve yields also $\beta = 0.30$. The results of β obtained with both methods are naturally in agreement.

In order to measure the static exponent ν and the dynamic exponent z in the pinning state for $H < H_c$, we take $H_c = 0.28$ and $\beta = 0.30$ as input, and adjust the values of ν and z to collapse the data according to the dynamic scaling form in Eq. (6). As is shown for the regime of $H < H_c$ in Fig. 3(b), the corresponding critical exponents are estimated to be $\nu = 1.3$ and $z = 2.4$.

The critical exponents are crucial identifications of the universality classes [46,48], which depend on the mechanism of dynamics, the structure of systems, the dimension of spins, etc. The depinning phase transition is usually of second-order for the QEW equation, Ising model, and ϕ^4 theory [25,26,29,33,49]. The numerical values of the static exponents are reported to be $\beta = 0.25$ and $\nu = 1.33$ for the 2D QEW equation [49], $\beta = 0.30$ and $\nu = 1.02$ for the 2D random-field Ising model with a driving field [29], and $\beta = 1.06$ and $\nu = 0.70$ for the 2D random-field ϕ^4 theory [33]. In our paper, we explore a similar continuous phase transition in 1D nanowires. The Heisenberg model with an anisotropic energy governed

by the LLG equation is in a universality class different from those of the 2D QEW equation, 2D random-field Ising model with Monte Carlo simulation, and 2D random-field ϕ^4 theory governed by the Hamiltonian equation. Yet some values of the exponents are relatively close to each other.

In particular, the dynamic exponent $z = 2.4$ for the LLG equation is larger than that of the empirical models, e.g., compared with $z = 1.33$ for the DRFIM [29], $z = 1.43$ for the QEW equation [49], and $z = 1.95$ for the ϕ^4 theory [33]. Since the dynamic evolution is slow, the computer time for simulating the LLG equation is several orders of magnitude longer than that for the Ising model. To obtain more accurate values of the critical driving field and critical exponents, the maximum evolution time of the domain wall motion should be extended to the scale of $t \sim 10^7$ or more. Hence, there is a requirement of more efficient numerical methods for simulations, and abundant computer resources in the further study of the phase transitions. Furthermore, the influence of anisotropic coefficients on the universality class remains an interesting but undeveloped topic.

To calculate the statistical fluctuation of the domain wall position, we define the fluctuation function,

$$\omega^2(t) = \langle h(t)^2 \rangle - \langle h(t) \rangle^2. \tag{7}$$

Here $\omega^2(t)$ includes the dynamic evolution of the background which may lead to a deviation from the scaling behavior in the very short-time regime. Therefore, we redefine a pure fluctuation function $D\omega^2(t)$ by subtracting the contribution of the background,

$$D\omega^2(t) = \omega^2(t) - \omega_b^2(t), \tag{8}$$

where $\omega_b^2(t)$ is actually the line susceptibility of the background computed from simulations starting from the fully ordered state without a domain wall. To further explore the influence
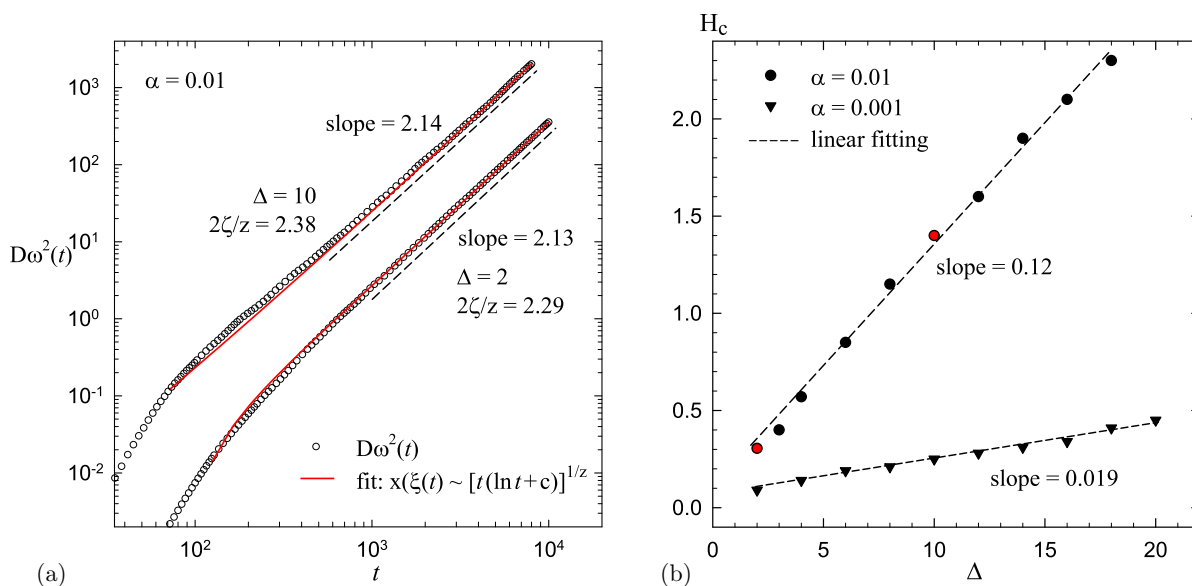
FIG. 4. (a) The pure fluctuation function $D\omega^2(t)$ is displayed for $\Delta = 2$ at $H_c = 0.28$ and $\Delta = 10$ at $H_c = 1.4$. The curve for $\Delta = 10$ is shifted up by a factor of 5 for clarity. The dashed lines indicate the direct measurements of slope, while the red solid lines represent the power-law fitting with logarithmic corrections to scaling, $c = 1.14$ for $\Delta = 10$ and $c = 5.01$ for $\Delta = 2$. (b) The transition field H_c is plotted for different disorder strengths, with $\alpha = 0.01$ denoted by circles and $\alpha = 0.001$ denoted by triangles. The two red circles correspond to the fluctuation analysis for $\Delta = 10$ and 2 in (a). The short dashed lines indicate the linear fittings. In both (a) and (b), $D_\perp = 4.23$.

of the bulk on the scaling behavior, we also perform the simulation from a completely disordered state. The result shows that $h(t)$ stabilizes at a constant value after a microscopic time for relaxation, therefore the contribution of the bulk can be neglected in Eq. (8).

At the transition point $\tau = 0$ and for a sufficiently long nanowire, the scaling analysis of the pure fluctuation function yields

$$D\omega^2(t) \sim t^{2\zeta/z}, \tag{9}$$

where ζ is similar to the roughness exponent in the 2D magnetic systems and describes the strength of the statistical fluctuation. A direct measurement of the slope from Fig. 4(a) gives $2\zeta/z = 2.13$ for $\Delta = 2$, and $2\zeta/z = 2.14$ for $\Delta = 10$. With the logarithmic correction to scaling, i.e., $\xi(t) \sim [t(\ln t + c)]^{1/z}$, the results are refined to $2\zeta/z = 2.29$ with $c = 5.01$ and $2\zeta/z = 2.38$ with $c = 1.14$, thus $\zeta = 2.75$ and 2.86, respectively.

In Fig. 4(b), the phase transition field H_c is plotted for different strengths of the random fields with the damping factor $\alpha = 0.001$ and 0.01. The phase transition field increases with the disorder augment almost linearly. This relation is similar to that of the 2D random-field Ising model, and the 2D clock model with quenched disorder [31].

V. SUMMARY

In summary, we have investigated the domain wall dynamics in magnetic nanowires governed by the LLG equation. In the absence of quenched disorder, we focus on the numerical solution below and above the Walker breakdown threshold. To understand the underlying behavior of the domain wall motion in the periodic breathing mode for $H > H_{\text{WB}}$, we theoretically deduce the expression of the oscillation period by introducing the biaxial anisotropy coefficients, and numerically verify how the period is controlled by the driving field, damping and hard anisotropy.

More importantly, we analyze the dynamic effects of quenched disorder, and detect a pinning-depinning phase transition of the domain wall motion in nanowires. For different strengths of the driving field H, the dynamic system exhibits the pinning and depinning phases below and above a critical driving filed H_c. We perform the dynamic scaling form analysis, and show the data collapse in the two phases. The critical driving filed H_c is linearly dependent on the strength of the disorder. In the depinning phase for $H > H_c$, the domain wall velocity reaches a constant after a microscopic time scale, the static critical exponent β is determined to be 0.30. According to the data collapse for $H < H_c$, another static exponent and the dynamic exponent are estimated to be $\nu = 1.3$ and $z = 2.4$.

Finally, we emphasize that if the quenched disorder is introduced to the quasi-1D, -2D, or -3D magnetic systems, the domain wall motion may be different from the 1D model as mentioned in Sec. II [17,38]. The dynamic effects of the quenched disorder destroy the homogeneity of the magnetic materials. For a cylindrical quasi-1D or -2D system, the uniformity in the perpendicular directions of the domain wall motion is disturbed by the disorder, hence the self-similarity in these directions is absent. We are working on further research of the phase transition on cylindrical and 2D magnetic systems, which will be described elsewhere.

[1] S. S. P. Parkin, M. Hayashi, and L. Thomas, Science **320**, 190 (2008).

[2] S. Krause, G. Herzog, T. Stapelfeldt, L. Berbil-Bautista, M. Bode, E. Y. Vedmedenko, and R. Wiesendanger, Phys. Rev. Lett. **103**, 127202 (2009).

[3] D. A. Allwood, G. Xiong, C. C. Faulkner, D. Atkinson, D. Petit, and R. P. Cowburn, Science **309**, 1688 (2005).

[4] N. L. Schryer and L. R. Walker, J. Appl. Phys. **45**, 5406 (1974).

[5] H. B. Braun, Adv. Phys. **61**, 1 (2012).

[6] A. Mougin, M. Cormier, J. P. Adam, P. J. Metaxas, and J. Ferré, Europhys. Lett. **78**, 57007 (2007).

[7] T. Ono, H. Miyajima, K. Shigeto, K. Mibu, N. Hosoito, and T. Shinjo, Science **284**, 468 (1999).

[8] S. Glathe, R. Mattheis, and D. V. Berkov, Appl. Phys. Lett. **93**, 072508 (2008).

[9] Y. Nakatani, A. Thiaville, and J. Miltat, Nat. Mater. **2**, 521 (2003).

[10] M. Yan, C. Andreas, A. Kákay, F. García-Sánchez, and R. Hertel, Appl. Phys. Lett. **99**, 122505 (2011).

[11] H. Forster, T. Schrefl, D. Suess, W. Scholz, V. Tsiantos, R. Dittrich, and J. Fidler, J. Appl. Phys. **91**, 6914 (2002).

[12] R. Wieser, U. Nowak, and K. D. Usadel, Phase Transitions **78**, 115 (2006).

[13] M. Kläui, J. Phys. Condens. Matter **20**, 313001 (2008).

[14] X. S. Wang, P. Yan, Y. H. Shen, G. E. W. Bauer, and X. R. Wang, Phys. Rev. Lett. **109**, 167209 (2012).

[15] X. S. Wang and X. R. Wang, Phys. Rev. B **90**, 184415 (2014).

[16] Z. Z. Sun and X. R. Wang, Phys. Rev. Lett. **97**, 077205 (2006).

[17] D. G. Porter and M. J. Donahue, J. Appl. Phys. **95**, 6729 (2004).

[18] D. Sander, R. Skomski, C. Schmidthals, A. Enders, and J. Kirschner, Phys. Rev. Lett. **77**, 2566 (1996).

[19] M. Kläui, H. Ehrke, U. Rüdiger, T. Kasama, R. E. Dunin-Borkowski, D. Backes, L. J. Heyderman, C. A. F. Vaz, J. A. C. Bland, G. Faini, E. Cambril, and W. Wernsdorfer, Appl. Phys. Lett. **87**, 102509 (2005).

[20] L. K. Bogart, D. Atkinson, K. O'Shea, D. McGrouther, and S. McVitie, Phys. Rev. B **79**, 054414 (2009).

[21] A. Kunz and J. D. Priem, IEEE Trans. Magn. **46**, 1559 (2010).

[22] H. Y. Yuan and X. R. Wang, Phys. Rev. B **89**, 054423 (2014).

[23] M. Jost, J. Heimel, and T. Kleinefeld, Phys. Rev. B **57**, 5316 (1998).

[24] P. J. Metaxas, J. P. Jamet, A. Mougin, M. Cormier, J. Ferré, V. Baltz, B. Rodmacq, B. Dieny, and R. L. Stamps, Phys. Rev. Lett. **99**, 217208 (2007).

[25] A. B. Kolton, A. Rosso, T. Giamarchi, and W. Krauth, Phys. Rev. Lett. **97**, 057001 (2006).

[26] S. Bustingorry, A. B. Kolton, and T. Giamarchi, Europhys. Lett. **81**, 26005 (2007).

[27] M. L. Trobo, E. V. Albano, and K. Binder, Phys. Rev. E **90**, 022406 (2014).

[28] U. Nowak and K. D. Usadel, Europhys. Lett. **44**, 634 (1998).

[29] N. J. Zhou and B. Zheng, and Y. Y. He, Phys. Rev. B **80**, 134425 (2009).

[30] N. J. Zhou and B. Zheng, Phys. Rev. E **90**, 012104 (2014).

[31] X. P. Qin, B. Zheng, and N. J. Zhou, Phys. Rev. E **86**, 031129 (2012).

[32] L. Wang, B. Zheng, and N. J. Zhou, Europhys. Lett. **107**, 16001 (2014).

[33] R. H. Dong, B. Zheng, and N. J. Zhou, Europhys. Lett. **99**, 56001 (2012).

[34] J. Leliaert, B. V. de Wiele, A. Vansteenkiste, L. Laurson, G. Durin, L. Dupré, and B. V. Waeyenberge, J. Appl. Phys. **115**, 233903 (2014).

[35] S. Fukami, M. Yamanouchi, S. Ikeda, and H. Ohno, Nat. Commun. **4**, 2293 (2013).

[36] T. J. Hayward, Sci. Rep. **5**, 13279 (2015).

[37] D. Bang and H. Awano, J. Appl. Phys. **115**, 17D512 (2014).

[38] R. Wieser, U. Nowak, and K. D. Usadel, Phys. Rev. B **69**, 064401 (2004).

[39] P. Landeros, O. J. Suarez, A. Cuchillo, and P. Vargas, Phys. Rev. B **79**, 024404 (2009).

[40] H. Kurebayashi, O. Dzyapko, V. E. Demidov, D. Fang, A. J. Ferguson, and S. O. Demokritov, Nat. Mater. **10**, 660 (2011).

[41] R. Wieser, E. Y. Vedmedenko, and R. Wiesendanger, Phys. Rev. B **81**, 024405 (2010).

[42] A. Thiaville, Y. Nakatani, J. Miltat, and N. Vernier, J. Appl. Phys. **95**, 7049 (2004).

[43] X. P. Wang, C. J. García-Cervera, and E. Weinan, J. Comput. Phys. **171**, 357 (2001).

[44] Y. Fily, E. Olive, N. Di Scala, and J. C. Soret, Phys. Rev. B **82**, 134519 (2010).

[45] W. Kleemann, Annu. Rev. Mater. Res. **37**, 415 (2007).

[46] M. F. Torres and R. C. Buceta, J. Stat. Mech. (2015) P10015.

[47] B. Zheng, Int. J. Mod. Phys. B **12**, 1419 (1998).

[48] H. H. Boltz and J. Kierfeld, Phys. Rev. E **90**, 012101 (2014).

[49] E. E. Ferrero, S. Bustingorry, and A. B. Kolton, Phys. Rev. E **87**, 032122 (2013).